

Preparation, Characterisation and Photocatalytic Activity of La-doped ZnO Nanopowders Synthesised using Auto-combustion

Mukhtar Ahmad^{ab*}, Eijaz Ahmed^a, Muhammad Ikram^a, Zhanglian Hong^b, Abdul Hafeez^c,
Khalid Nadeem Riaz^d, Fezza Zafar^a, Niaz Ahmed Niaz^a and Waqar Ahmed^{ef}

^aDepartment of Physics, Bahauddin Zakariya University, Multan 60800, Pakistan

^bState Key Laboratory of Silicon Materials, Department of Materials Science & Engineering,
Zhejiang University, Hangzhou 310027, China

^cScience and Technology Division, University of Education, Lahore, Pakistan

^dDepartment of Physics, University of Gujrat, Gujrat 50700, Pakistan

^eInstitute of Nanotechnology and Bioengineering, University of Central Lancashire, School of Medicine,
Preston PR1 2HE, United Kingdom

^fDentistry and School of Pharmacy, Preston PR1 2HE, United Kingdom

(received August 18, 2014; revised August 9, 2015; accepted August 18, 2015)

Abstract. Nanocrystalline nanoparticles of pristine ZnO and La-doped ZnO have been synthesised using a combustion method using various concentrations of lanthanum dopant followed by calcination for 3 h at 700 °C. The crystalline structure, chemical composition and optical characteristics have been characterised using X-ray diffraction (XRD), scanning electron microscopy (SEM) attached with energy dispersive X-ray (EDX) spectroscopy, Brunauer Emmett Teller (BET), UV-vis. spectroscopy and photoluminescence (PL) spectroscopy. Absorption spectra showed that the absorbance increased with La-doping and the blue shift observed was due to an increase in the band gap from 3.24 to 3.27 eV. The photocatalytic activities of the samples prepared were evaluated using the photocatalytic degradation of methyl orange (MO) under irradiation by sunlight. The textile mill effluents containing organic matter were also irradiated with sunlight inducing photocatalysis and the chemical oxygen demand (COD) of the treated effluent were investigated. The results showed that the ZnO photocatalyst doped with 1.0 at.% lanthanum exhibited four times enhancement in the photocatalytic activity compared to pure ZnO.

Keywords: ZnO, combustion, XRD, photocatalysis, methyl orange, La-doped ZnO

Introduction

Fabrication and characterisation of semiconducting nanostructured materials have received considerable attention over the last few years due to increasing influence on our everyday life (Suwanboon and Amornpitoksuk, 2011; Wang and Herron, 1991). Zinc oxide (ZnO) has attracted interest due to its photocatalytic ability useful for the degradation of environmental pollutants and is attractive alternative to TiO₂ as a photoactive catalyst (Kaneva *et al.*, 2011; Anandan *et al.*, 2007). ZnO has exhibited superior performance with lower cost compared to TiO₂ in degrading organic dyes in acidic and basic media. It has a hexagonal wurtzite structure with an *n*-type conductivity (Reddy *et al.*, 2011; Chen *et al.*, 1998). The structural, optical, electrical and physical properties of ZnO nanoparticles and the effects of doping on these properties have been studied earlier by several researchers (Ahmad *et al.*, 2013; Shinde *et al.*, 2006; Ismail *et al.*, 2001). Dramatic

*Author for correspondence; E-mail: mzkhm73@gmail.com

changes in the electrical and optical properties of ZnO and unique properties due to doping have been observed by Bouderbala *et al.* (2008). Due to its useful properties, ZnO has been used in photocatalytic applications (Xiao *et al.*, 2015; Zhou *et al.*, 2009). ZnO is an ideal catalyst in photocatalysis since it is nontoxic with holes of strong oxidising power and being inexpensive (Peng *et al.*, 2007). When ZnO nanoparticle is illuminated with a light of appropriate wavelength, the valence band potential is positive enough to generate hydroxyl radicals at the surface, and the conduction band potential is negative enough to reduce molecular O₂. The hydroxyl radical is a powerful oxidising agent and can attack organic pollutants present at or near the surface of the ZnO to degrade it. However, the photocatalytic efficiency at the present stage is still very low, which is mainly caused by the fast recombination of photogenerated electron-hole pairs during photocatalysis. Thus, further improving the photocatalytic efficiency is still a major challenge in the research field of photocatalysis until

now. Therefore, for enhancing photocatalytic activity of ZnO, doping of metal or nonmetal ions is a useful technique (Abed *et al.*, 2015; Elangoran *et al.*, 2015). Metal doping induces localized states between the valence band and the conduction band. These mid-gap states could trap temporarily the photogenerated electron-hole pairs, thus suppress the recombination of charge carriers (Wan *et al.*, 2015; Zhao *et al.*, 2015). Recent research has been focused on the doping of ZnO by lanthanide ions with 4f electron configuration. Lanthanide ions can form complexes with various Lewis bases including organic acids, amines, aldehydes, alcohols, and thiols by the interaction of the functional groups with their f-orbital (Ahmad *et al.*, 2015). Thus, doping lanthanide ions into a ZnO matrix could provide a means to concentrate organic pollutants on the semiconductor surface and therefore, can improve the separation efficiency of photo-induced electron-hole pairs of ZnO to enhance the photoreactivity (Ahmad *et al.*, 2015; Ciciliati *et al.*, 2015).

In this study, pure ZnO and La-doped ZnO using the auto-combustion technique has been synthesised producing highly pure nanocrystalline powders with large surface area at relatively low temperatures (Hwang and Wu, 2004). Variations in the properties of ZnO powders were studied as a function of the lanthanum dopant concentrations.

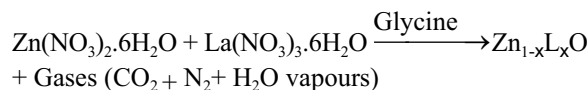
Materials and Methods

Synthesis of undoped and La-doped ZnO nanopowders. Pure and La-doped ZnO nanopowders were synthesised using the combustion technique. Zinc nitrate ($\text{Zn}(\text{NO}_3)_2 \cdot 6\text{H}_2\text{O}$) and glycine ($\text{NH}_2\text{CH}_2\text{COOH}$) were used as starting reagents. The zinc nitrate served as a source of zinc and as an oxidising agent whereas glycine acted as a fuel (Ahmad *et al.*, 2013).

Precursor formation. For pure ZnO, homogeneous mixture of glycine and zinc nitrate was obtained by mixing them together in the optimised molar ratio (Ahmad *et al.*, 2012a) through magnetic stirring. This resulted in the formation of transparent slurry by absorbing moisture from air due to the hygroscopic nature of zinc nitrate. The slurry was then dehydrated at 130 °C to obtain precursor using a hot plate.

Auto-ignition. The precursor was heated at 200 °C to cause precursor ignition. During combustion the evolution of gases occurred with generation of heat. Heat treatment at 700 °C was done for 3 h resulting in

the liberation of gases and formation of dry, crystalline white ZnO powders. For the preparation of La-doped ZnO samples, lanthanum nitrate [$\text{La}(\text{NO}_3)_3 \cdot 6\text{H}_2\text{O}$] was added to the initial mixture of zinc nitrate and glycine. Rest of the process was similar to that used for pure ZnO. The following chemical reaction occurs during the synthesis of La-doped ZnO samples:



Characterisation. Powder X-ray diffraction (XRD) patterns of as-synthesised ZnO and La-doped ZnO samples were recorded using a Rigaku Dmax-III A X-ray diffractometer with Ni filtered $\text{Cu K}\alpha$ radiation source. The surface morphology, particle size and compositional analysis of photocatalysts were examined using a scanning electron microscope (Hitachi S-4800) with EDX and transmission electron microscope (JEOL JEM 1200EX) and X-ray photoelectron spectroscopy (XPS, VG ESCALAB MARK II) with a monochromatic $\text{Mg K}\alpha$ X-ray source. Specific surface areas of samples were determined using Brunauer Emmett Teller (BET) surface area analyzer (NOVA 2200e Quantachrome, USA) using nitrogen as a purge gas. UV-vis diffuse reflectance spectra (DRS) were measured in the range of 380–460 nm using a Hitachi U-4100 UV-vis spectrometer. PL emission spectra were recorded using Hitachi F-4500 fluorescence spectrophotometer. The sample excitation was made at 325 nm at room temperature.

Measurement of photocatalytic activity. Photocatalytic activities of ZnO and La-doped ZnO nanopowders were estimated by monitoring the degradation of methyl orange (MO) as a model compound in a self-assembled apparatus under natural sunlight radiation source. In this study, photocatalytic activities under natural sunlight were investigated. The peak at 464 nm was used to monitor the photocatalytic degradation of MO. For the photocatalytic experiment, 50 mg photocatalysts were suspended in MO aqueous solution (50 mL) with a concentration of 20 mg/L in a beaker. The suspension was magnetically stirred for 30 min to reach the adsorption/desorption equilibration without light exposure. This was followed by a photocatalytic reaction started by the exposure of the desired light. The temperature of the suspension was kept at about 20 °C by an external cooling jacket with recycled water. After a setup exposure time, 5 mL suspension was sampled, centrifuged and the supernatant was taken out for uv-

vis absorption spectrum measurement. The intensity of the main absorption peak of the MO dye was referred to as the measure of the residual dye concentration.

Analytical method. Total organic carbon (TOC) content was measured after the degradation of model dye in the presence of the photocatalysts under sunlight irradiation (Mukherjee, 2011). After photodegradation, the total organic carbon content of model dye was observed to decrease with time. The decrease of carbon content indicates the degradation of the organic dye into nontoxic decomposed compounds. Moreover, the mineralisation of substrate was measured by chemical oxygen demand (COD) reduction method. Chemical oxygen demand of textile effluent was estimated before and after the photocatalytic treatment with a standard dichromate method, using COD digester. Arsenic effluent was diluted to facilitate light penetration through solution and the initial COD of diluted effluent was 412 mg/L. The amount of catalysts was 50 mg/25 mL and an average intensity of sunlight was 1.20×10^5 lux during the photocatalytic measurements. The percentage photodegradation efficiency (η) was calculated from the following expression:

$$\eta = \left[\frac{\text{COD}_i - \text{COD}_f}{\text{COD}_i} \right] \times 100$$

Where:

COD_i = before treatment

COD_f = after treatment

All the experiments were performed under the same experimental conditions such as sunlight irradiation (between 9 am and 3 pm), constant temperature, pH and photocatalyst load etc.

Results and Discussion

XRD analysis. Figure 1 shows powder X-ray diffraction patterns of pure ZnO and La-doped ZnO as a function of lanthanum dopant concentrations. The physical characteristics such as crystallite size and unit cell parameters are presented in Table 1. The strong and sharp peaks existing in the XRD spectra show the presence of wurtzite structure of ZnO. The strong peaks are located at an angle (2θ) of 31.7° , 34.4° and 36.2° correspond to (1 0 0), (0 0 2) and (1 0 1) along with the other peaks which are found at the angles of 47.5° , 56.6° , 62.9° , 66.4° , 67.9° , 69.2° , 72.7° and 77.0° correspond to (1 0 2), (1 1 0), (1 0 3), (2 0 0), (1 1 2), (2 0 1), (0 0 4) and (2 0 2) planes, which all are found

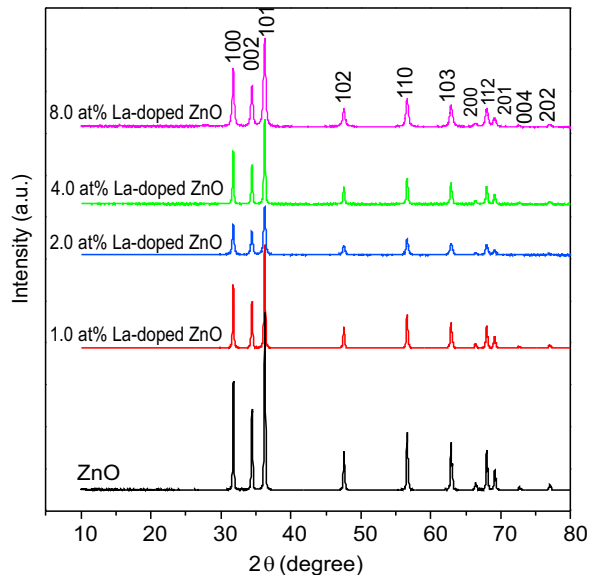


Fig. 1. X-ray diffraction patterns of pure ZnO and La-doped ZnO sample

Table 1. Crystallite size and unit cell parameters of pure ZnO and La-doped ZnO sample.

Photocatalysts	Crystallite size (nm)	Lattice parameters	
		'a' (Å)	'c' (Å)
Pure ZnO	27	3.254	5.208
1.0 at.% La-doped ZnO	24	3.258	5.203
2.0 at.% La-doped ZnO	22	3.262	5.199
4.0 at.% La-doped ZnO	23	3.263	5.195
8.0 at.% La-doped ZnO	19	3.265	5.186

in correspondence to those given in JCPDS 05-0664 and previous studies (Ghouri *et al.*, 2014; Ahmad *et al.*, 2013). The diffraction patterns of La-doped ZnO were similar to the undoped ZnO showing that lanthanum doping in ZnO did not affect its crystal structure. This also indicates that La^{3+} is uniformly dispersed on ZnO nanoparticles in the form of small La_2O_3 cluster (Anandan *et al.*, 2007). The observed peaks for La-doped ZnO, however, are wider with the width increasing with increasing La-content. La-doping caused a random variation in diffraction peak intensities. Intensity decreased up to 2.0 at% La-content and then increased. The change in the intensity and width of the observed diffraction peaks as a function of La-content is attributed to the decrease in the crystallite size (Suwanboon and

Amornpitoksuk, 2011; Flickyngerova *et al.*, 2008; Anandan *et al.*, 2007), which goes on changing inversely with change in La concentration. Lattice parameters 'a' and 'c' were estimated using the formula:

$$\left[\frac{1}{d_{hkl}} \right]^2 = \frac{4}{3} \left[\frac{h^2 + k^2 + hk}{a^2} \right] + \frac{1}{c^2}$$

Lattice parameters and crystallite size variation as functions of La-content were calculated. The calculated values of lattice parameters 'a' and 'c' are 3.254 Å and 5.208 Å while for 2.0 at.% La-doped ZnO are 3.262 Å and 5.199 Å, respectively. Lattice parameters increased with increase in La-content which is obvious as ionic radius of Zn⁺² is 0.074 nm and that of La⁺³ is 0.106 (Suwanboon and Amornpitoksuk, 2011) and lattice parameters should expand if ionic radius of the dopant is greater as compared to Zn ions (Dole *et al.*, 2011). Average crystallite sizes were estimated using the full width at half maximum (FWHM) of highly intense diffraction peak in Debye-Scherrer's formula (Culity and Stock, 2001).

$$t = \frac{0.9\lambda}{\beta \cos\theta}$$

Average crystallite size estimated for pure ZnO to be 27 nm which decreases up to 19 nm with increase in La-content. It is interesting to note that the particle size of La doped ZnO is smaller as compared with that of the pure ZnO. The decrease in the particle size of La-doped ZnO is mainly attributed to the formation of La–O–Zn on the surface of the doped samples, which hinders the growth of crystal grains (Korake *et al.*, 2014; Jia *et al.*, 2009; Anandan *et al.*, 2007).

SEM, EDX and TEM. Figure 2(a-d) displays the surface morphology of pure ZnO and 2.0 at% La-doped ZnO nanopowders. SEM micrographs of pristine ZnO nanopowders exhibited clusters of tiny particles, whilst 2.0 at% La-doped ZnO nanopowders revealed flakes of ultrafine particles with voids or holes. The high porosity in the nanopowders could be attributed to the liberation of large amount of gaseous products such as H₂O vapours, CO₂ and N₂ during combustion process (Ahmad *et al.*, 2013b). TEM images in Fig. 2, show that, for undoped ZnO nanopowders, the particles are spherical and larger and, while for 2.0 at% La-doped ZnO nanopowders, they are smaller and quasi spherical. Lanthanum doping thus changes the morphology of the

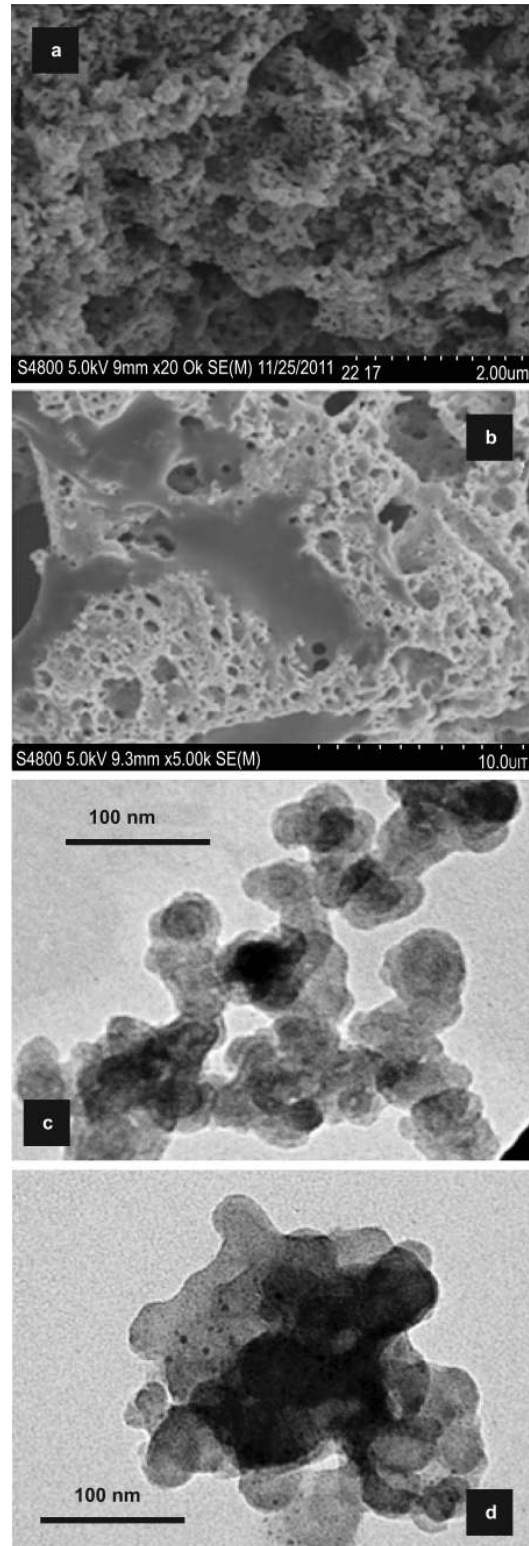


Fig. 2. (a-d) SEM micrograph of (a) pure ZnO and (b) 2.0 at% La-doped ZnO samples; TEM images of (c) pure ZnO and (d) 2.0 at% La-doped ZnO sample.

final product. TEM investigations of all of the samples revealed that the crystallites are of nanometer size. The diameter of ZnO and 2.0 at% La-doped ZnO were found to be about 33 and 24 nm, respectively agreeing with the XRD results. The chemical compositional analysis is important for monitoring the concentration of the dopant. Figure 3 shows the EDX spectra of undoped ZnO and La-doped ZnO nanoparticles. The EDX spectrum of the La-doped ZnO displays a clear lanthanum line at 4.65 keV showing La doping. No traces of other elements were found in the spectra which confirm the purity of the samples. Also Table 2 shows the atomic percentage of Zn, La and O for undoped and La-doped ZnO samples. Here the actual concentration of La is found to be 1.76 at% for 2.0 at% La-doped ZnO sample.

XPS analysis. The nature and the co-ordination of the elements present in the La-doped ZnO were investigated by X-ray photoelectron spectroscopy (XPS). The La 3d spectrum of 2.0 at% La-doped ZnO is shown in Fig. 4.

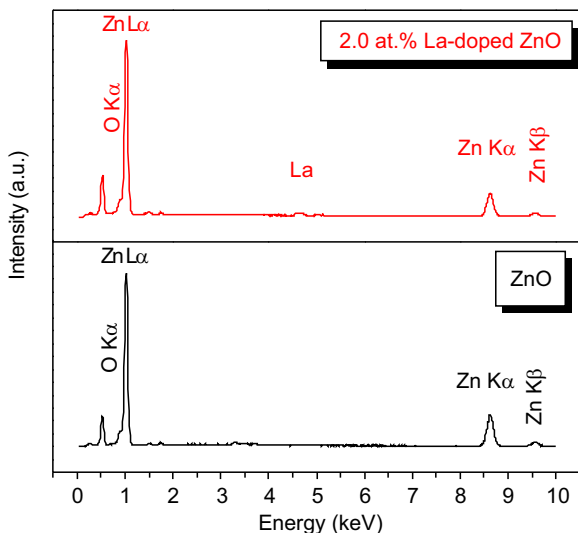


Fig. 3. EDX pattern of ZnO and 2.0 at%La-doped ZnO sample.

Table 2. Chemical composition (atomic % of ZnO and La-doped ZnO sample).

Element	Zn (at%)	O (at%)	La (at%)	Total (at%)
ZnO	50.68	49.32	-	100
2.0 at% La-doped ZnO	48.73	49.51	1.76	100

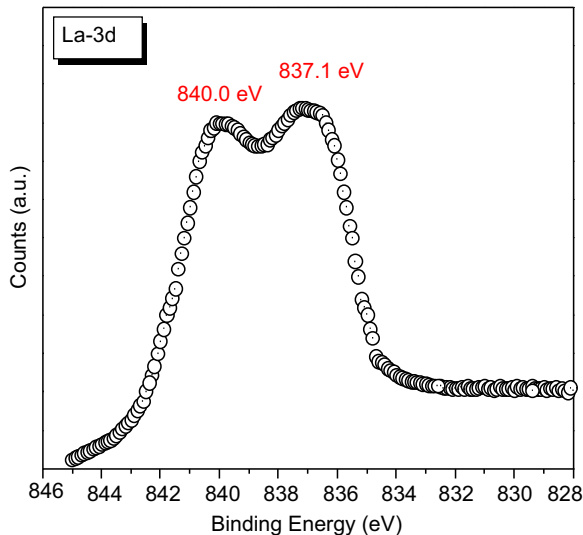


Fig. 4. XPS high resolution spectra of La-3d region for 2 at% La- ZnO sample.

The spectrum exhibits two components with the binding energy values of 837.1 eV and 840.0 eV. The highest energy contribution is assigned to the bonding between lanthanum and zinc while the lowest energy contribution is attributed to the bonding in the lanthanum oxide clusters (Anandan *et al.*, 2007). These results demonstrated that the bonding between the lanthanum and zinc has occurred and the interaction between the lanthanum oxide clusters and the ZnO surface are strongly developed.

UV-visible spectra. Optical properties of ZnO and La-doped ZnO photocatalysts with different La-content were measured by diffuse reflectance spectroscopy (DRS) at room temperature. The absorbance spectra of different samples are shown in Fig. 5. The band edge for the ZnO sample was appeared at about 387 nm while the band edges of the La-doped ZnO samples was shifted to shorter wavelength regions with higher absorption intensity after La-doping. The blue shift in wavelength is attributed to gradual increase in band gap of ZnO on La-doping. The absorbance coefficient (α) was calculated from the raw absorbance data to obtain the optical band gap (E_g). The band gap values were thus determined by the extrapolation of the linear portion of the $(\alpha h\nu)^2$ curve versus the photon energy $h\nu$ and are shown in Table 3. With increasing the La-content from 0.0 at% to 8.0 at%, the band gap energies increased in the range of 3.24-3.27 eV as shown in Fig. 6. The following explanation may be given; the band gap of ZnO is about 3.37 eV whereas that of La_2O_3 is about

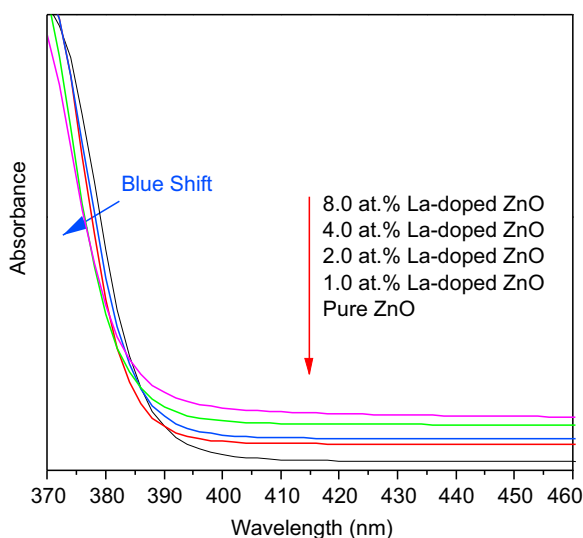


Fig. 5. Absorption spectra for pure ZnO and La-doped ZnO sample.

Table 3. Band gap energy, BET surface area of ZnO and La-doped ZnO samples and apparent kinetic values for the degradation MO model dye under sunlight irradiation

Photocatalyst	Band gap (eV)	BET surface area (m ² /g)	For sunlight irradiation	
			r ₀ (mg/L/min)	t _{1/2} (min)
ZnO	3.24	33.4	0.038	217
1.0 at.% La-doped ZnO	3.25	37.3	0.162	86
2.0 at.% La-doped ZnO	3.25	39.5	0.132	104
4.0 at.% La-doped ZnO	3.26	42.3	0.106	130
8.0 at.% La-doped ZnO	3.27	45.1	0.092	149

5.5 eV (Jia *et al.*, 2009), which is much higher than that of pure ZnO. An additional energy level could be formed above the conduction band of ZnO due to the La-doping. Furthermore, this could be attributed to the quantum size effect as well as the strong interaction between the surface oxides of Zn and La. These observations strongly suggest that the La doping significantly affects the particle size and hence the absorbance properties. Moreover, these results are in good agreement with the conclusion derived from the XRD results and a similar result has also been reported in La-doped TiO₂ by

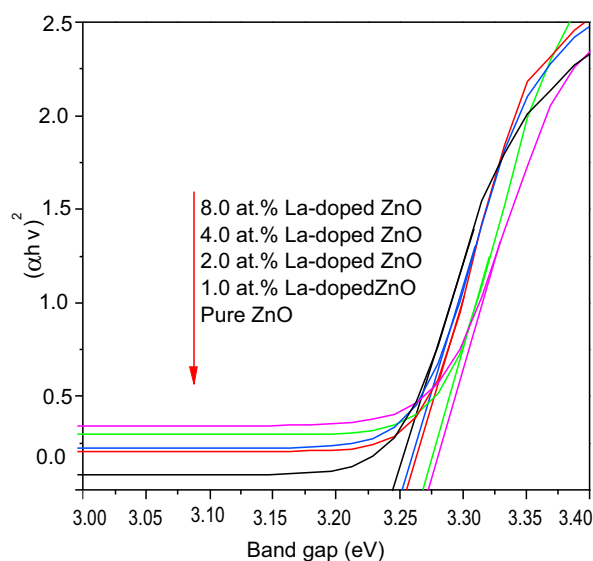


Fig. 6. Band gap energies of ZnO and La-doped ZnO sample.

Liqiang *et al.* (2004) and La-doped ZnO by Anandan *et al.* (2007).

Photoluminescence. Photoluminescence (PL) is a powerful tool to investigate optical properties of wide band gap semiconductors. A comparison of PL emission spectra intensity of prepared samples excited with 325 nm wavelengths ranging up to 600 nm is shown in Fig. 7. PL emission intensity decreased with La-concentration i.e. pure ZnO has highest emission

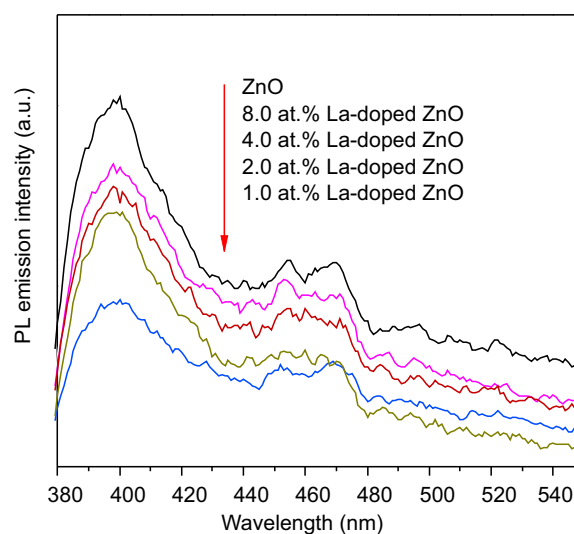


Fig. 7. PL emission spectra for pure ZnO and La-doped ZnO nanoparticles.

intensity, which can be attributed to several defects such as oxygen and zinc vacancies or oxygen and zinc interstitials (Ismail *et al.*, 2001). However, the addition of La ions tends to stop the reduction in the band gap resulting in lower PL emission intensity first and then increasing with increasing dopant La-content.

Photocatalytic activity. Pristine ZnO and doped ZnO are well known catalysts used in photocatalytic degradation of pollutants. Photocatalytic activities of the ZnO and La-doped ZnO samples were determined through a series of experiments carried out for degradation of methyl orange (MO) in aqueous suspension under natural sunlight irradiation. A blank experiment study of MO degradation without catalyst loading under the same condition was also observed. The results indicate that the mere photolysis can be ignored as the corresponding degradation is about 0.3% after irradiations for 2 h. Figure 8 shows a comparison of photocatalytic performances of pure ZnO and La-doped ZnO nanoparticles. About 9% of the MO was adsorbed for ZnO sample upon stirring for 30 min in the dark and increased for La-doped ZnO in comparison to ZnO nanopowders. The pronounced adsorption is due to increase in specific surface area, increase in porosity and defects creation within band gap by

lanthanum doping. Photocatalytic degradation of MO follows pseudo first-order reaction kinetics for low dye concentrations

$$\ln(C_0/C) = k_{app}t$$

where:

k_{app} = the apparent constant, used as the basic kinetic parameter for different photocatalysts; C_0 = the initial concentration of MO in aqueous solution and C = the residual concentration of MO at time t .

The initial degradation rate ($r_0=k_{app}C_0$) of 20 mg/L MO with different photocatalysts was studied and the results are presented in Table 3. The photodegradation rate of MO follows the ascending order; 1.0 at% La-doped ZnO > 2.0 at% La-doped ZnO > 4.0 at% La-doped ZnO > 8.0 at% La-doped ZnO > ZnO > commercial ZnO. The degradation rate under sunlight for 1.0 at% La-doped ZnO photocatalyst was found superior to other La-doped ZnO and ZnO samples. The specific surface areas were seen to increase gradually with the increasing lanthanum content (Table 3) enhancing the adsorption performance. The photocatalytic efficiency of La-doped ZnO mainly originates from the formation of La-O-Zn bonds on ZnO surface. Photocatalytic degradation rate of MO is observed to be lower under La-doped ZnO. Table 3 shows that the degradation rate of MO enhanced with La-content up to 1.0 at% La-content and then decreased with La-loading leading to the conclusion that 1.0 at% doping concentration is the optimum loading to ZnO that is more efficient in separating photoinduced electron-hole pairs which in turn increases photoactivity of ZnO. The high photocatalytic activity at 1.0 at% La-doped ZnO can be explained as follows: lanthanum ions in ZnO can result in the formation of a space charge layer on the surface of ZnO which acts as a barrier for recombination of photoinduced electron-hole pairs resulting in an increase in the photocatalytic activity. This increase was observed up to 1.0 at% La-doping in the present study. The decrease in photocatalytic activity of ZnO beyond 1.0 at% La-doping is justified as: The incorporation of lanthanum beyond 1.0 at% is supposed to likely result in the formation of more La-O-Zn bond on ZnO surface due to which surface charge region is negatively affected causing a decrease in its efficiency to separate the photoinduced electron-hole pairs and instead of acting as traps sites for photoinduced electron-hole pairs, it acts as recombination centre (Jia *et al.*, 2009). This results in decrease of photocatalytic activity of ZnO.

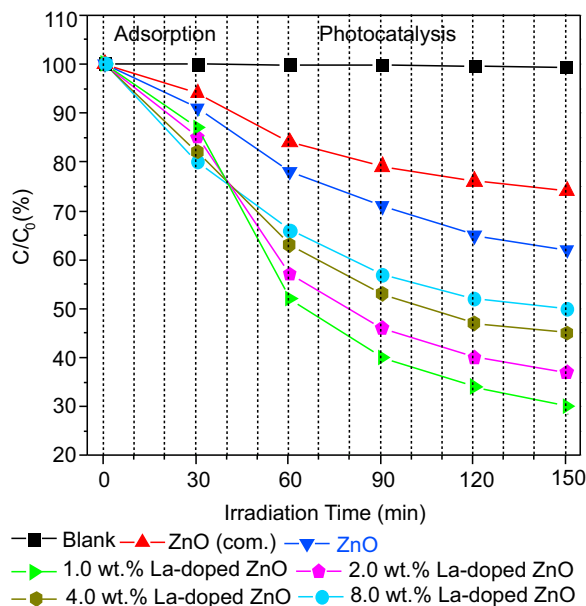


Fig. 8. Photocatalytic activity of pure ZnO, Commercial ZnO and La-doped ZnO nanopowders for MO degradation under sunlight irradiation.

A simple mechanism to understand the enhancement of photocatalytic activity of La-doped ZnO photocatalysts is the loading of lanthanum metals on the ZnO surface, which can accelerate the transport of photo-generated electrons to the outer systems. The transfer of electrons to the deposited metal causes these to become negatively charged (Behnajady *et al.*, 2009). In the photocatalytic systems, lanthanum deposited on the ZnO surface increased the photocatalytic activity by accelerating the transfer of electrons to dissolved oxygen molecules. Superoxide anion radical was prepared as a result of oxygen reduction by transfer of trapped electrons from lanthanum metal to oxygen. Consequently, the recombination of the photo-generated carriers were effectively suppressed leading to an increase in the photo-oxidation efficiency. The photocatalyst 1.0 at% La-doped ZnO exhibited superior catalytic performance, but further increase in the concentration of lanthanum would decrease photocatalytic activity because too much doping of lanthanum is likely to serve as recombination centre than as trap sites for the charge transfer at the interface. The total organic carbon (TOC) content was measured after the degradation of methyl orange dye in the presence of the photocatalysts under sunlight irradiation. After photodegradation the total organic carbon content of MO was observed to decrease with time and the results are presented in Fig. 9. TOC_0 and TOC_t are the initial

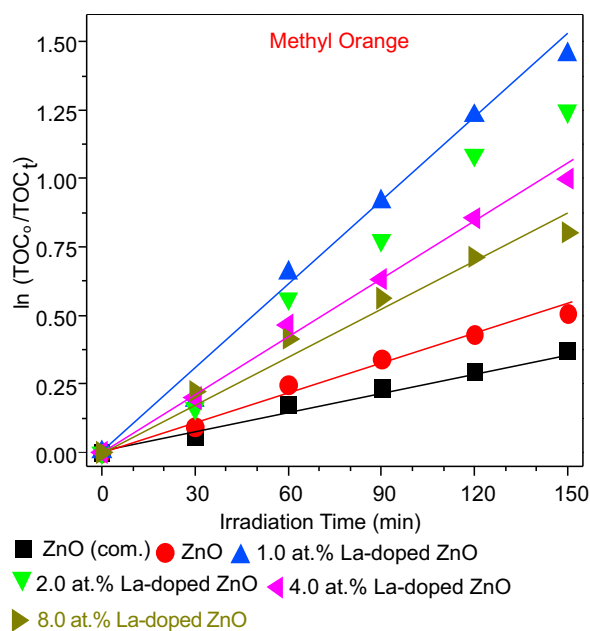


Fig. 9. The $\ln(TOC_0/TOC_t)$ vs time curves of mineralization of methyl orange.

concentration and the reaction concentration of MO, respectively. The experimental data are fitted using the pseudo-first-order kinetic equation.

During dye production and textile manufacturing processes an enormous amount of waste water containing dyestuffs with intensive colour and toxicity is introduced into the aquatic system. An effluent of this type has been considered for this photocatalytic degradation study using the same experimental conditions discussed in the experimental section. COD removal efficiencies of the effluent by ZnO, La-doped ZnO nanopowders

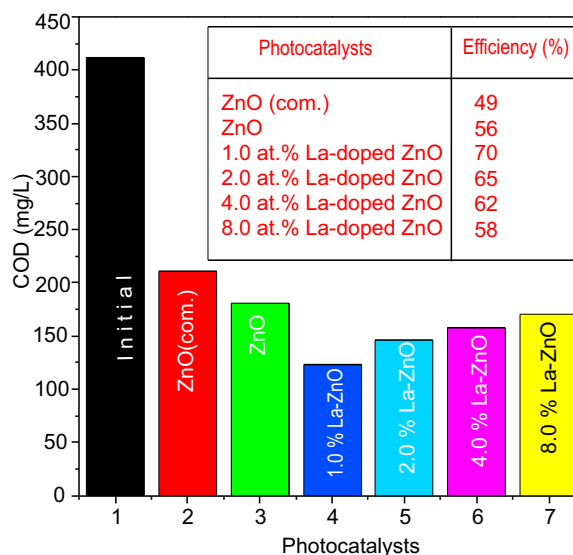


Fig. 10. COD values of the treated effluent and percentage photodegradation efficiency (η) for different photocatalysts under sunlight irradiation

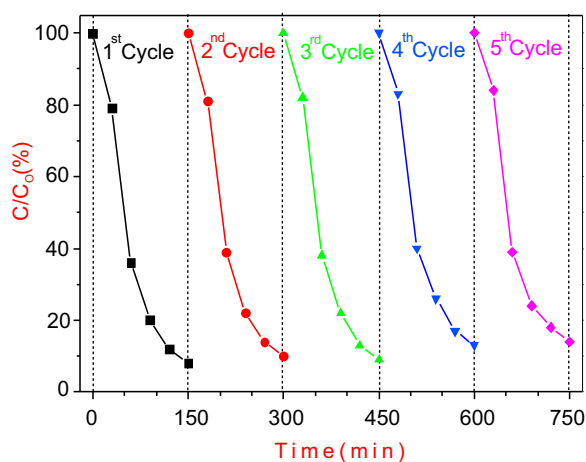


Fig. 11. Photo-stability of 1.0 at% La-doped ZnO sample.

photocatalysts under the sunlight irradiation are shown in Fig. 10. COD reduction confirms the destruction of the organic molecules in the effluents along with colour removal. The photo-stability of 1.0 at% La-doped ZnO sample as catalyst under sunlight was also studied (Fig. 11). The photocatalytic activity of the sample did not decrease significantly after five successive cycles of degradation tests, indicating that the photocatalyst was fairly stable under the conditions used in this study.

Conclusion

Pure ZnO and La-doped ZnO nanoparticles were synthesised via fast and facile conventional combustion method and characterised using a variety of characterisation techniques. From XRD patterns all synthesised samples had a hexagonal wurtzite structure showing that La-doping has no structural effect on ZnO. It was found that La^{3+} is uniformly dispersed on ZnO nanoparticles in the form of small La_2O_3 cluster. The XRD and UV-vis results revealed that the particle size of La-doped ZnO is much smaller as compared to that of pure ZnO and decreases with increasing La loading. Highly porous surface of La-doped ZnO was observed by SEM, which is critical for enhancing the adsorption and photocatalytic activity. The photocatalytic activity of La-doped ZnO for the degradation of MO was studied and the results are compared with ZnO and commercial ZnO. It was observed that the rate of degradation of MO over La-doped ZnO increases with increasing La loading up to 1.0 at% and then decreases. The TOC results demonstrated that La-doped ZnO requires shorter irradiation time for the complete mineralization of MO than pure ZnO. The relative photonic efficiencies and the photocatalytic activity of the 1.0 at% La-doped ZnO are much higher as compared to those of pure ZnO and commercial ZnO. It is concluded that, small particle size, separation of charge carriers, highly porous surface and larger specific surface area of La-doped ZnO are the major constituents for its enhanced photocatalytic activity in the present study.

Acknowledgement

Mukhtar Ahmad is thankful to Higher Education Commission (HEC) of Pakistan for providing financial assistance through Indigenous and IRSIP Scholarship Programme and the Zhejiang University of China for providing opportunity to work in its laboratories.

References

Abed, C., Bouzidi, C., Elhouichet, H., Gelloz, B., Ferid, M. 2015. Mn doping induced high structural quality of sol-gel ZnO crystals: Application in photo-

catalysis. *Applied Surface Science*, **349**: 855-863.

Ahmad, M., Ahmed, E., Zafar, F., Khalid, N.R., Niaz, N.A., Hafeez, A., Ikram, M., Khan, M.A., Hong, Z.L. 2015. Enhanced photocatalytic activity of Ce-doped ZnO nanopowders synthesized by combustion method. *Journal of Rare Earths*, **33**: 255-260.

Ahmad, M., Ahmed, E., Hong, Z.L., Iqbal, Z., Khalid, N.R., Abbas, T., Ahmad, I., Elhissi, A., Ahmed, W. 2013. Structural, optical and photocatalytic properties of hafnium doped zinc oxide nanophotocatalyst. *Ceramic International*, **39**: 8693-8700.

Ahmad, M., Ahmed, E., Hong, Z.L., Khalid, N.R., Zhang, Y., Ullah, M. 2013a. Preparation of highly efficient Al doped ZnO photocatalyst by combustion synthesis. *Current Applied Physics*, **13**: 697-704.

Ahmad, M., Iqbal, Z., Hong, Z., Yang, J., Zhang, Y., Khalid, N.R., Ahmed, E. 2013b. Enhanced sunlight photocatalytic performance of hafnium doped ZnO nanoparticles for methylene blue degradation. *Integrated Ferroelectrics*, **145**: 108-114.

Ahmad, M., Ahmed, E., Hong, Z.L., Khalid, N.R., Elhissi, E., Ahmed, W. 2013c. Graphene-Ag/ZnO nanocomposite as a high performance photocatalyst under visible light irradiation. *Journal of Alloys and Compounds*, **577**: 717-727.

Ahmad, M., Ahmed, E., Khalid, N.R., Jackson, M.J., Ahmed, W. 2012a. Synthesis and characterization of hexagonal shaped nanocrystalline zinc oxide powders. *International Journal of Manufacturing Materials and Mechanical Engineering*, **2**: 61-76.

Ahmad, M., Ahmed, E., Hong, Z.L., Khalid, N.R. 2012b. Effect of fuel to oxidant molar ratio on the photocatalytic activity of ZnO nanopowders. *Ceramic International*, **39**: 3007-3015.

Anandan, S., Vinu, A., Lovely, K.L.P.S., Gokulakrishnan, N., Srinivasu, P., Mori, T., Murugesan, V., Sivamurugan, V., Ariga, K. 2007. Photocatalytic activity of ZnO for the degradation of monocrotophos in aqueous suspension *Journal of Molecular Catalysis A: Chemical*, **266**: 149-157.

Behnajady, M.A., Modirshahla, N., Shokri, M., Zeininezhad, A., Zamani, H.A. 2009. Enhancement photocatalytic activity of ZnO nanoparticles by silver doping with optimization of photo-deposition method parameters. *Journal of Environmental Science: Health Part A*, **44**: 666-672.

Bouderbala, M., Hamzaoui, S., Amrani, B., Reshak, A.H., Adnane, M., Sahraoui, T., Zerdali, M. 2008. Thickness dependence of structural, electrical and optical behaviour of undoped ZnO thin films. *Physica B: Condensed Matter*, **403**: 3326-3330.

Chen, Y.F., Bagnall, D.M., Koh, H.J., Park, K.T., Hiraga,

- K.J., Zhu, Z.Q., Yao, T.F. 1998. Plasma assisted molecular beam epitaxy of ZnO on c-plane sapphire-growth and characterization. *Journal of Applied Physics*, **84**: 3912-3918.
- Ciciliat, M.A., Silva, M.F., Fernandes, D.M., de Melo, M.A.C., Hechenleitnar, A.A.W., Pineda, E.A.G. 2015. Fe-doped ZnO nanoparticles: Synthesis by a modified Sol-gel method and characterization. *Materials Letters*, **159**: 84-86.
- Culity, B.D., Stock, S.R. 2001. *Elements of X-ray Diffraction*, 3rd edition., pp. 388 Prantice-Hall Inc., New Jersey, USA.
- Dole, B.N., Mote, V.D., Huse, V.R., Purushotham, Y., Lande, M.K., Jadhav, K.M., Shah, S.S. 2011. Structural studies of Mn doped ZnO nanoparticles. *Current Applied Physics*, **11**: 762-766.
- Elangoran, S.V., Chandramohan, V., Sivakumar, N., Senthil, T.S. 2015. Synthesis and characterization of sodium doped ZnO nanocrystals and its applications to photocatalysis. *Superlattices and Microstructures*, **85**: 901-907
- Flickyngerova, S., Shtereva, K., Stenova, V., Hasko, D., Novotny, I., Tvarozek, V., Sutta, P., Vavrinsky, E. 2008. Structural and optical properties of sputtered ZnO thin films. *Applied Surface Science*, **254**: 3643-3647.
- Ghouri, M.I., Ahmad, E., Khalid, N.R., Ahmad, M., Ramzan, M., Shakoor, A., Niaz, N.A. 2014. Gadolinium doped ZnO nanocrystalline powders and its photocatalytic performance for degradation of methylene blue under sunlight. *Journal of Ovonic Research*, **10**: 89-100.
- Hwang, C.C., Wu, T.Y. 2004. Synthesis and characterization of nanocrystalline ZnO powders by a novel combustion synthesis method. *Materials Science and Engineering B*, **111**: 197-206.
- Ismail, B., Abaab, M., Rezig, B. 2001. Structural and electrical properties of ZnO films prepared by screen printing technique. *Thin Solid Films*, **383**: 92-94.
- Jia, T., Wang, W., Long, F., Fu, Z., Wang, H., Zhang, Q. 2009. Fabrication characterization and Photocatalytic tivity of La-doped ZnO nanowires. *Journal of Alloys and Compounds*, **484**: 410-415.
- Kaneva, N.V., Dimitrov, D.T., Dushkin, C.D. 2011. Effect of nickel doping on the photocatalytic activity of ZnO thin films under UV and visible light. *Applied Surface Science*, **257**: 8113-8120.
- Korake, P.V., Dhabbe, R.S., Kadam, A.N., Gaikwad, Y.B., Garadkar, K.M. 2014. Highly active lanthanum doped ZnO nanorods for photodegradation of metasytox. *Journal of Photochemistry and Photobiology B: Biology*, **130**: 11-19.
- Liqiang, J., Xiaojun, S., Baifu, X., Baiqi, W., Weimin, C., Honggang, F. 2004. The preparation and characterization of La-doped TiO₂ nanoparticles and their photocatalytic activity. *Journal of Solid State Chemistry*, **177**: 3375-3382.
- Mukherjee, D. 2011. Development of a Novel TiO₂-Polymeric Film Photocatalyst for Water Purification both under UV and Solar Illumination. *Ph.D. Thesis*, 143 pp., University of Western Ontario, Canada.
- Peng, F., Zhu, H., Wang, H., Yu, H. 2007. Preparation of Ag-sensitized ZnO and its photocatalytic performance under simulated solar light. *Korean Journal of Chemical Engineering*, **24**: 1022-1026.
- Reddy, A.J., Kokila, M.K., Nagabhushana, H., Rao, J.L., Shivakumara, C., Nagabhushana, B.M., Chakradhar, R.P.S. 2011. Combustion synthesis, characterization and Raman studies of ZnO nanopowders. *Spectrochimica Acta Part A*, **81**: 53-58.
- Shinde, V.R., Gujar, T.P., Lokhande, C.D., Mane, R.S., Han, S.H. 2006. Mn doped and undoped ZnO film: A comparative structural, optical and electrical properties study. *Materials Chemistry and Physics*, **96**: 326-330.
- Suwanboon, S., Amornpitoksuk, P. 2011. Preparation and characterization of nanocrystalline La-doped ZnO powders through a mechanical milling and their optical properties. *Ceramics International*, **37**: 3515-3521.
- Wan, X., Liang, X., Zhang, C., Li, X., Liang, W., Xu, H., Lan, S., Tie, S. 2015. Morphology controlled synthesis of Cu-doped ZnO, tubular Zn(Cu)O and Ag decorated tubular Zn(Cu)O microcrystals for photocatalysis. *Chemical Engineering Journal*, **272**: 58-68.
- Wang, Y., Herron, N. 1991. Nanometre-sized semiconductor cluster: Material synthesis, quantum size effects, and photophysical properties. *Journal of Physical Chemistry*, **95**: 525-532.
- Xiao, S., Li, H., Liu, L., Lian, J. 2015. Glucose-assisted generation of assembled mesoporous ZnO sheets with highly efficient photocatalytic performance. *Materials Science in Semiconductor Processing*, **39**: 680-685.
- Zhao, T., Fu, Y., Zhao, Y., Xing, L., Xue, X. 2015. Gd-doped ZnO nanowire nanogenerator as self-powered/active humidity sensor with high sensitivity and fast response. *Journal of Alloys and Compounds*, **648**: 571-576
- Zhou, X., Li, Y., Peng, T., Xie, W., Zhao, X. 2009. Synthesis, characterization and its visible-light-induced photocatalytic property of carbon doped ZnO. *Materials Letters*, **63**: 1747-1749.